Supporting Information

Silica spheres-directed N-doped carbon supported Ni catalysts boost electrochemical CO evolution for syngas production

Chaofan Zhang and Zhongkui Zhao*

State Key Laboratory of Fine Chemicals, Department of Catalysis Chemistry and Engineering, School of Chemical Engineering, Dalian University of Technology, Dalian 116024 (P. R. China)

E-mail: zkzhao@dlut.edu.cn.

Experimental Section

Preparation of SiO_2 (80 nm): 10 g of deionized water, 58.5 g of anhydrous ethanol, and 1 g of $NH_3 \cdot H_2O$ were added into a 200 mL round-bottom flask. After stirring at 30 °C for 30 min, 5.3 g of tetraethyl orthosilicate (TEOS) was added to the above solution. The mixture was kept static at 30 °C for 1 h, followed by centrifugation, washing, and drying to obtain 80 nm SiO_2.

Preparation of SiO_2 (260 nm): 10 g of deionized water, 58.5 g of anhydrous ethanol, and 4 g of $NH_3 \cdot H_2O$ were added into a 200 mL round-bottom flask. After stirring at 30 °C for 30 min, 5.3 g of tetraethyl orthosilicate (TEOS) was added. The mixture was maintained at 30 °C for 1 h, then subjected to centrifugation, washing, and drying to afford 260 nm SiO_2.

Preparation of SiO_2 (430 nm): 25 mL of deionized water, 50 mL of anhydrous ethanol, and 7.5 mL of $NH_3 \cdot H_2O$ were mixed uniformly under stirring in a 250 mL beaker. Then, 15 mL of tetraethyl orthosilicate (TEOS) was added dropwise slowly. After stirring at room temperature for 5 h, the product was collected by centrifugation, washed, and dried to obtain 430 nm SiO_2.

Preparation of Ni/NC-D: 0.1 g of glucose, 0.5 g of dicyandiamide, and 0.5 g of NH_4Cl were dissolved in 20 mL of deionized water under stirring. Subsequently, 10 mg of $NiCl_2 \cdot 6H_2O$ was added, and the solution was stirred for 10 min. Then, 0.75 g of 80 nm of SiO_2 was introduced, and stirring was continued for 12 h. After rotary evaporation, the obtained powder was ground uniformly and transferred into an Al_2O_3 crucible. Carbonization was performed in a tube furnace at 900 °C for 2 h under a N_2 flow of 40 mL min^{-1} with a heating rate of 3 °C min^{-1}. After cooling to room temperature, the product was immersed in 40 mL of 2 M NaOH solution and kept at 80 °C for 12 h to etch away SiO_2. The solid was collected by suction filtration, washed to neutrality, and dried to obtain Ni/NC-80. The Ni/NC-260 and Ni/NC-430 samples were prepared by using the similar preparation process to that of Ni/NC-80 except for the replacement of SiO_2 sphere (80 nm) by those with 260 nm and 430 nm diameters, respectively. According to our previous work,[1] the Ni/NC was prepared by the similar process to that of Ni/NC-80 except for the absence of hard template. For comparison, the corresponding NC support of the Ni/NC-260 catalyst was prepared by using the similar process to that of Ni/NC-260 except for the absence of Ni precursor.

Working Electrode Preparation: The catalyst ink was prepared by dispersing 5 mg of catalyst in a mixture of 100 μL isopropanol, 300 μL water, and 10 μL of a 5 wt% Nafion solution, followed by ultrasonication for 1 h. Then, 80 μL of the resulting ink was drop-cast onto a 1×1.5 cm carbon paper (HCP030P) and dried to obtain the working electrode. The catalyst loading area was 1 cm^2, corresponding to a mass loading of 1.0 mg cm^{-2}.

Electrochemical Measurements: All electrochemical experiments were performed using a CHI 660e electrochemical workstation in an H-cell electrolyzer, separated by a Nafion 117 membrane. Prior to use, the proton exchange membrane was pretreated by boiling in 5 wt% H_2O_2 for 1 h, followed by rinsing and soaking in deionized water for 0.5 h. Subsequently, it was treated with 0.5 M H_2SO_4 at 80 °C for 1 h, followed by another rinsing and soaking step in deionized water for 0.5 h. The electrolyte used was 40 mL of 0.5 M $KHCO_3$. An Ag/AgCl electrode (saturated with KCl) and a carbon rod were used as the reference and counter electrodes, respectively. The catalyst-coated carbon paper served as the working electrode. All measured potentials were converted to the reversible hydrogen electrode (RHE) scale using the equation: *E* (V vs. RHE) =*E* (V vs. Ag/AgCl) + 0.0591 × pH + 0.197.

Before performance testing, the catholyte was saturated by purging with Ar/CO_2 (15 mL/min). Catalyst activation/conditioning was first carried out by performing cyclic voltammetry (CV) scans in the potential range of 0 to -1.2 V vs. RHE until stable curves were obtained. Linear sweep voltammetry (LSV) was then conducted from 0 to -1.0 V vs. RHE at a scan rate of 5 mV/s. The electrochemical active surface area (ECSA) was evaluated by measuring the double-layer capacitance (Cdl), which was determined from CV curves obtained in the non-Faradaic potential region of 0.65 to 0.75 V vs. RHE at various scan rates.

Product Analysis: CO_2 was continuously fed into the cathode compartment at a flow rate of 15 mL/min during electrolysis. After saturation, controlled-potential electrolysis (i-t curve) was performed by applying specific potentials to the working electrode. The gas products were quantified using a gas chromatograph (GC 9790) equipped with a thermal conductivity detector (TCD) and a flame ionization detector (FID). Liquid products were analyzed by ^{1}H NMR spectroscopy using dimethyl sulfoxide (DMSO) as an internal standard. The Faradaic efficiency of both CO or H_2 production resulting from the electrolysis were calculated as follow:

$$FE_{gaseous}\% = \frac{Q_i}{Q_{total}} * 100\% = \frac{Z_i * P_0 * V_0 * v(vol\%) * F}{R * T * I * 60\left(s\ min^{-1}\right)} =$$

$$\frac{2 * 1.013 * 10^5(Pa) * V_0\left(mL\ min^{-1}\right) * 10^{-6}\left(m^3\ mL^{-1}\right) * v(vol\%) * 96485\ \left(C\ mol^{-1}\right)}{8.314\ \left(m^3\ Pa\ mol^{-1}\ K^{-1}\right) * 298\ (K) * I\ \left(Cs^{-1}\right) * 60\left(s\ min^{-1}\right)}$$

Here, Z_i is the number of electrons needed for reducing CO_2 to H_2 or CO. Both H_2 and CO need 2 electrons, P_0 is the pressure, V_0 is the gas flow rate measured by a flow meter, v (vol%) is the volume ratio of H_2 or CO in the GC sampling loop, F is the Faradaic constant (96485 C·mol^{-1}), R is the ideal gas constant (8.314 m^3 Pa·mol^{-1}·K^{-1}), T is the reaction temperature (298 K), and I is the average current of the chronoamperometry curve.

Characterization of catalysts: X-ray diffraction (XRD) was performed by Rigaku Corporation

SmartLab 9 operated at 40 kV and 40 mA with Cu Kα radiation. Scanning electron microscope (SEM) were taken by NOVA Nano SEM 450. X-ray photoelectron spectroscopy (XPS) was obtained using a ESCALAB 250Xi XPS system equipped with Al Kα X-ray source. The N_2 adsorption-desorption isotherms were measured by Beishide instrument. The CO_2-TPD was measured by chemical adsorption analyzer (PCA1200).

Supplementary Figures

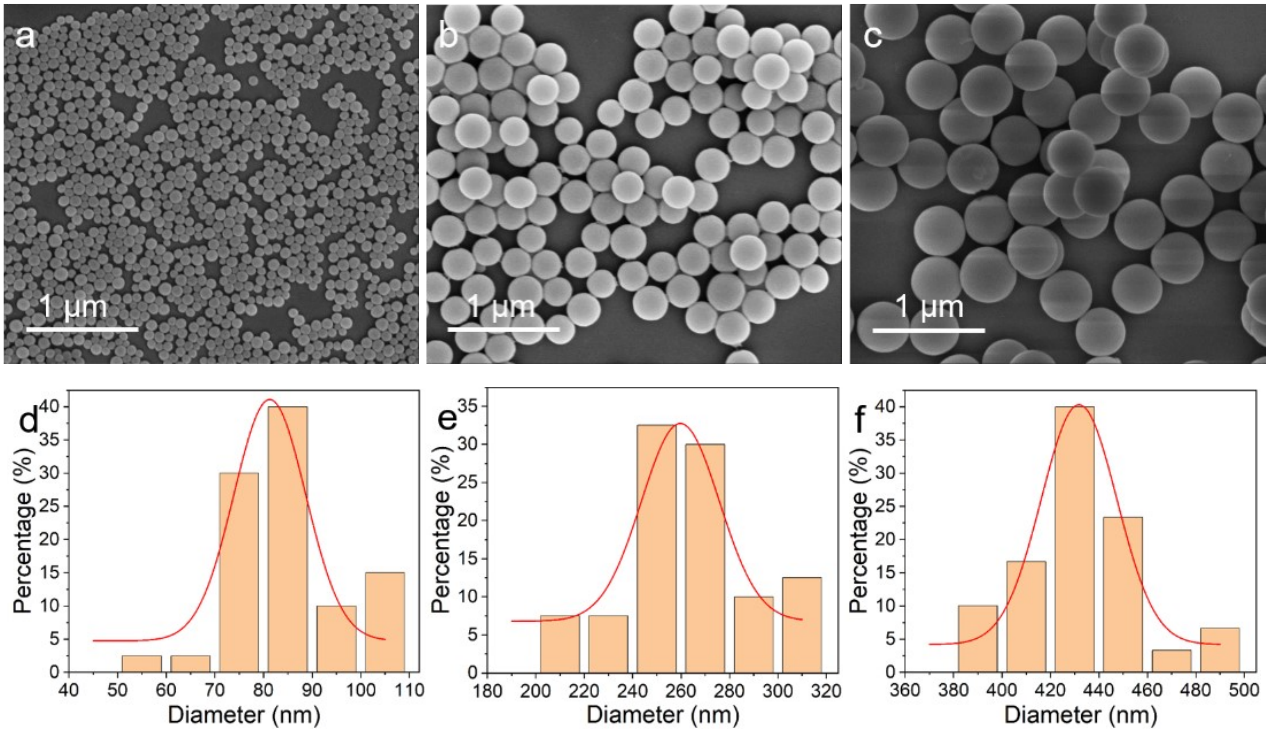

Fig. S1. SEM images (a-c) and corresponding size distribution plots (d-f) of SiO_2 microspheres with various sizes.

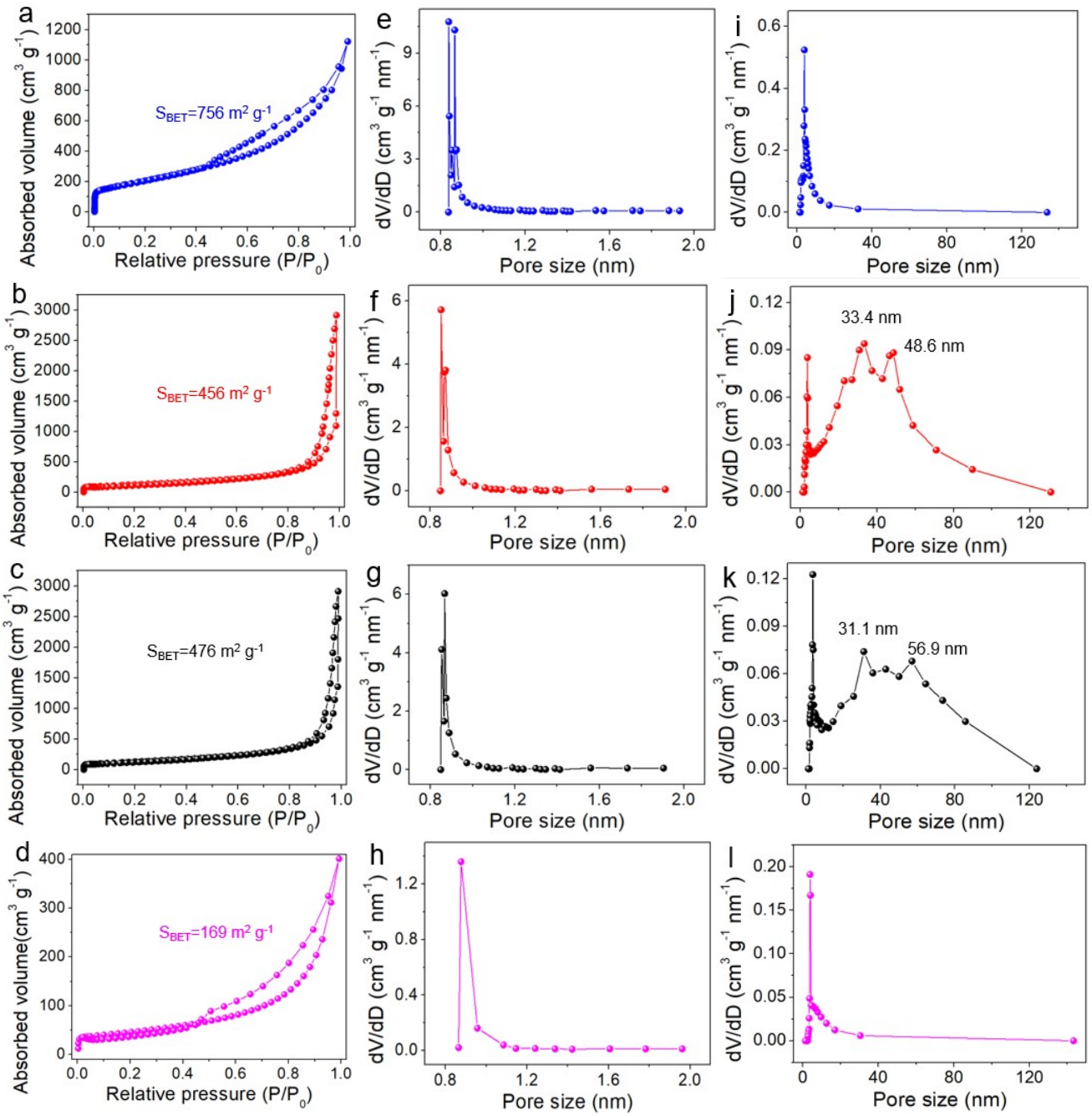

Fig. S2. a-d) N_2 adsorption-desorption isotherms of Ni/NC-80 (a), Ni/NC-260 (b), Ni/NC-430 (c) and Ni/NC (d). e-h) The micropore size distributions of Ni/NC-80 (e), Ni/NC-260 (f), Ni/NC-430 (g) and Ni/NC (h) by the H-K mode. i-l) The BJH pore size distributions of Ni/NC-80 (i), Ni/NC-260 (j), Ni/NC-430 (k) and Ni/NC (l) from the desorption branches.

N_2 adsorption-desorption experiments were performed to determine the textural properties of samples. From Fig. S2 and Table S1, in comparison with the supported Ni catalysts on the NC carrier prepared in the absence of silica template (Ni/NC, 756 m^2 g^{-1} and 0.621 cm^3 g^{-1}), all of the three Ni/NC-D catalysts show higher specific surface area (756, 456, and 476 m^2 g^{-1} for Ni/NC-80, Ni/NC-260, and Ni/NC-430, respectively) and total pore volume (1.735,

4.507, and 4.506 cm^3 g^{-1} for Ni/NC-80, Ni/NC-260, and Ni/NC-430, respectively). The results highlight the critical role of the silica template in constructing porous structures (Fig. S2a-d). Besides the micropores, much more mesopores on all of the silica spheres-templated Ni/NC-D catalysts and even macropores on Ni/NC-260 and Ni/NC-430 with larger pore volume have been obtained, owing to the changed gas-template effect of the released gas during the pyrolysis of mixture composed of glucose, dicyandiamide, and NH_4Cl by the adjusted size of silica spheres. In comparison with the Ni/NC-80, Ni/NC-260 shows a smaller specific surface area while possessing a larger pore volume, ascribed to the modulated pyrolysis process of precursors by the changed size of the SiO_2 sphere. The size of hard template can change the pyrolysis process of the precursors of carbon and nitrogen. By adopting the same mass ratio of the precursors of carbon and nitrogen to silica template, the larger sized silica template would lead to thicker accumulation of the precursors of carbon and nitrogen, subsequently result in more mesopores and macropores but less micropores by the gas template through the released gas from the pyrolysis of precursors of carbon and nitrogen as well as NH_4Cl (Table S1). The more micropores within Ni/NC-80 endows it with larger surface area than Ni/NC-260. Moreover, the large of amount of as-formed mesopores and macropores within Ni/NC-260 increase the total pore volume. The as-formed hierarchically porous structures would accelerate mass transfer.

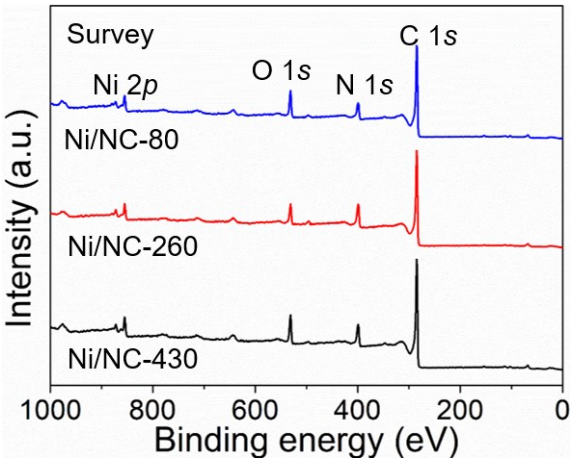

Fig. S3. The XPS survey spectra of Ni/NC-80, Ni/NC-260 and Ni/NC-430.

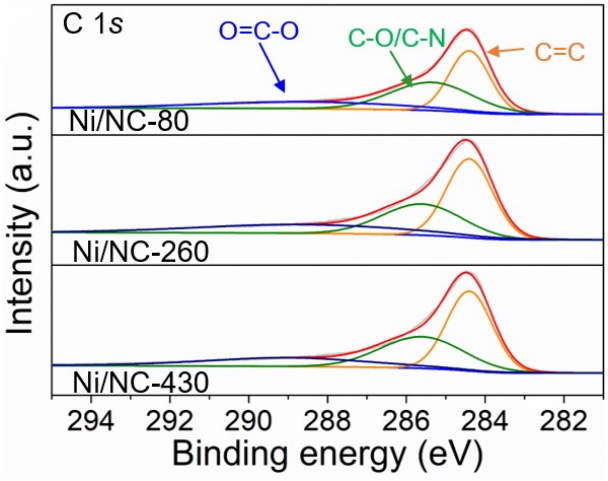

Fig. S4. The C 1s xps spectra of Ni/NC-80, Ni/NC-260 and Ni/NC-430.

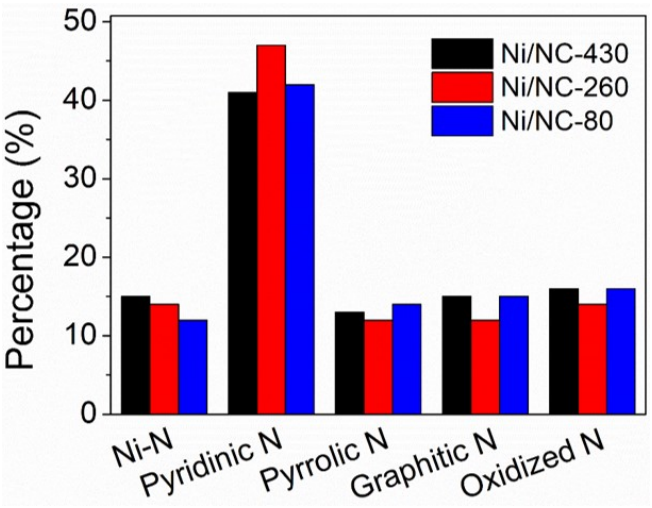

Fig. S5. Content of different types of N in Ni/NC-80, Ni/NC-260 and Ni/NC-430.

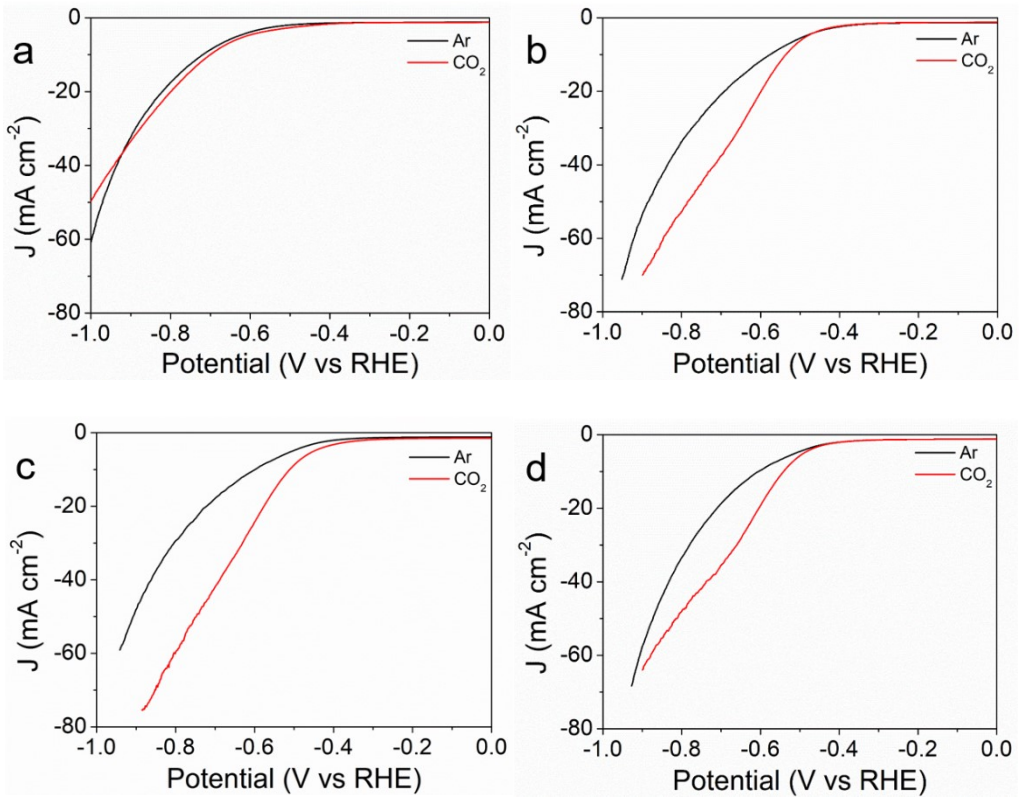

Fig. S6. a-d) LSV curves in Ar or CO_2-saturated 0.5 M $KHCO_3$ solution with a scan rate of 5 $mV \cdot s^{-1}$ of NC (a), Ni/NC-80 (b), Ni/NC-260 (c) and Ni/NC-430 (d).

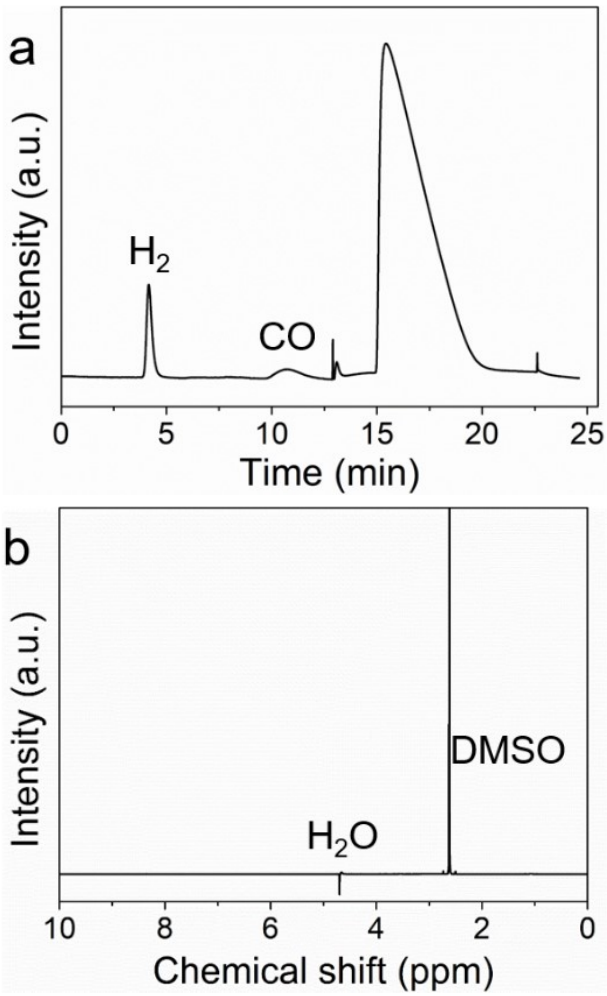

Fig. S7. a,b) Gas chromatograms (a) and ^{1}H NMR spectrum (b) of CO_2RR products over Ni/NC-260.

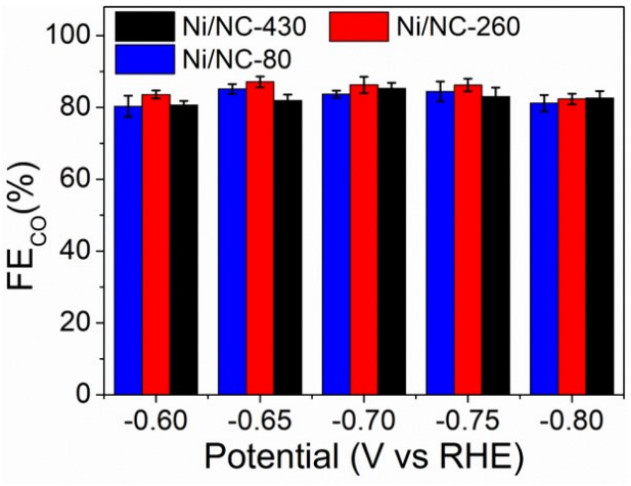

Fig. S8. The FE_{CO} of Ni/NC-80, Ni/NC-260 and Ni/NC-430.

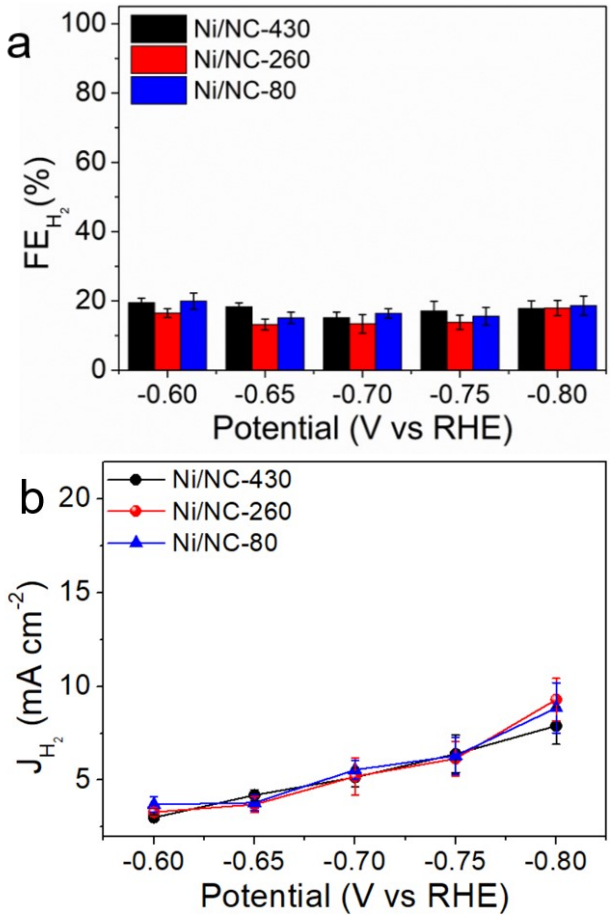

Fig. S9. a-b) The FE_{H2} (a) and J_{H2} (b) of Ni/NC-80, Ni/NC-260 and Ni/NC-430.

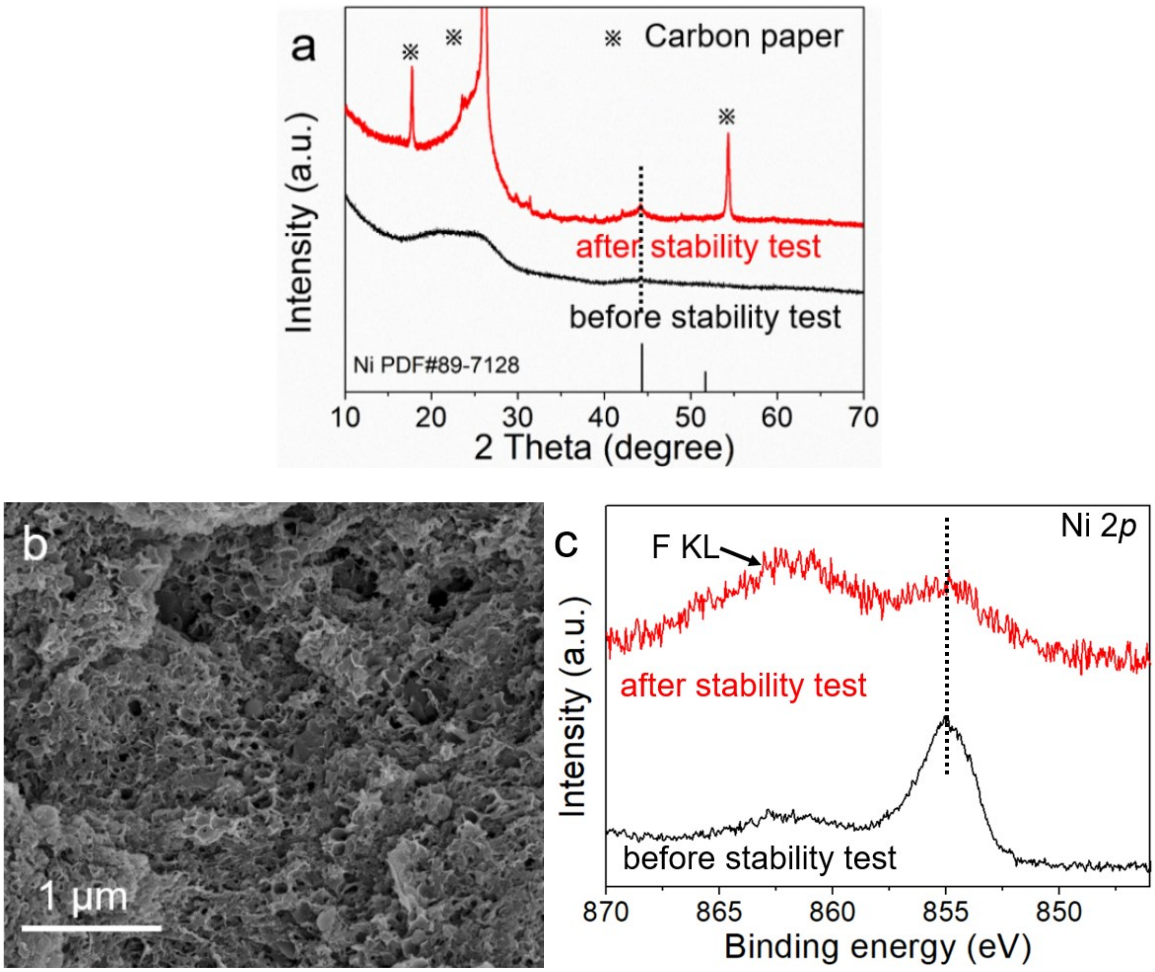

Fig. S10. Characterization of the Ni/NC-260 catalysts after stability testing at -0.65 V vs RHE (a) XRD, (b) SEM and (c) Ni 2*p* XPS spectrum.

Post-reaction characterizations reveal no obvious structural or chemical changes after electrolysis. The XRD patterns remain essentially unchanged compared with the fresh sample (Fig. S10a), while SEM images show that the porous structure is well preserved without noticeable collapse or aggregation (Fig. S10b). In addition, the Ni 2*p* XPS spectra exhibit negligible changes after cycling (Fig. S10c), suggesting that the chemical state of Ni species is maintained during the reaction process.

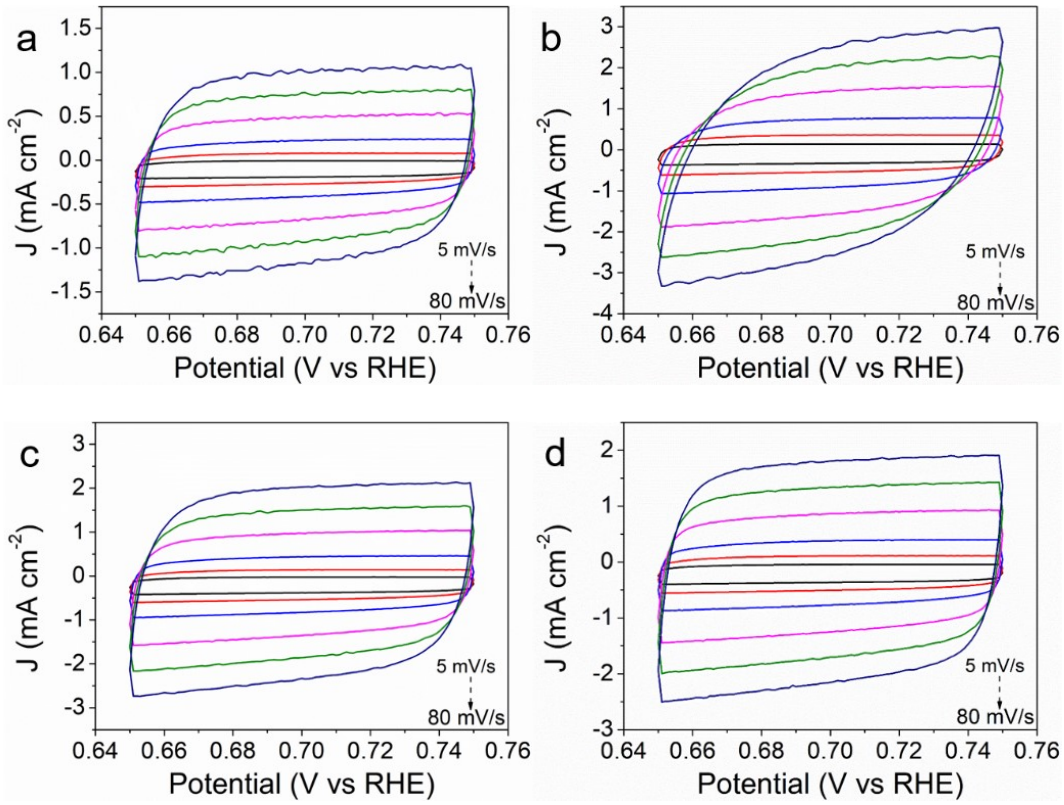

Fig. S11. a-d) CV curves of NC (a), Ni/NC-80 (b), Ni/NC-260 (c) and Ni/NC-430 (d) under different scan rates from 5 mV·s^{-1} to 80 mV·s^{-1}.

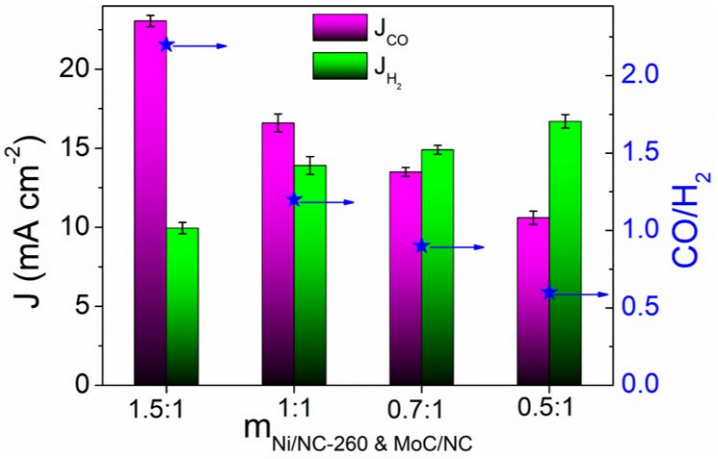

Fig. S12. J_{CO}, J_{H2}, and CO/H_2 ratios for the electrocatalytic CO_2RR for syngas production over the Ni/NC-260&MoC/NC composite catalysts including PCE and PHE units with a diverse mass ratios of Ni/ NC-260 to MoC/NC (1.5:1, 1:1,0.7:1 and 0.5:1).

The CO/H_2 ratios of Ni/NC-260 & MoC/NC with mass ratios of 1.5:1, 1:1, 0.7:1, and 0.5:1 are 2.2, 1.2, 0.9, and 0.6, with corresponding J_{CO} values of 23.1, 16.6, 13.5, and 10.6 mA cm^{-2}, respectively, further demonstrating that varying the mass ratio continuously adjusts the relative contributions of CO_2RR and HER.

Supplementary Tables

Table S1. BET surface area and the pore volume of Ni/NC-80, Ni/NC-260, Ni/NC-430 and Ni/NC.

Samples	S_{BET}[a] (m^2 g^{-1})	Pore volume (cm^3 g^{-1})		
		V_{Total}[b]	$V_{Micropor.}$[c]	$V_{Mesopor./Macropor.}$[d]
Ni/NC-80	756	1.735	0.307	1.428
Ni/NC-260	456	4.507	0.187	4.320
Ni/NC-430	476	4.506	0.193	4.313
Ni/NC	160	0.621	0.069	0.552

[a]Specific surface area, determined by the Brunauer-Emmett-Teller (BET) method. [b]Total pore volume, determined from the adsorbed volume at a single point of P/P0 at 0.99. [c]Microporous volume, derived from DFT analysis. [d]Mesoporous/macroporous volume, calculated by substracting DFT microporous volume from total pore volume.

Table S2. Electrocatalytic CO_2RR performance of the catalysts in the H-type cell.

Catalysts	E (V vs RHE)	J_{CO} (mA cm^{-2})	Electrolyte	Ref.
Ni/NC	-0.8	35.4	0.5 M $KHCO_3$	1
Ni_6@Ni-N_3	-1.0	43.5	0.5 M $KHCO_3$	2
Ni@NCNT/HPNF-3.4	-1.0	24.7	0.5 M $KHCO_3$	3
Br-Ni/NC	-0.96	48.0	0.5 M $KHCO_3$	4
Ni_{NP}/Ni_{SA} -N-C	-0.95	42.7	0.5 M $KHCO_3$	5
Ni@N-C	-1.0	21.8	0.5 M $KHCO_3$	6
Ni_2-N_3-C_4	-0.88	23.7	0.5 M $KHCO_3$	7
Ni_3-NC	-0.8	48.9	0.5 M $KHCO_3$	8
NC@Ni/C-60	-1.45	42.0	0.5 M $KHCO_3$	9
L-Ni-NC-C	-1.0	15.0	0.1 M $KHCO_3$	10
Ni-DACs	-1.0	56.4	0.5 M $KHCO_3$	11
Ni-N-HCNs	-1.1	41.9	0.5 M $KHCO_3$	12
Ni@GNRs	-1.1	44	0.5 M $KHCO_3$	13
Ni-NC(HPU)	-0.8	24.7	0.5 M $KHCO_3$	14
NiNG-S	-0.9	40.3	0.1 M $KHCO_3$	15
Ni-NC-NS	-1.0	18.1	0.5 M $KHCO_3$	16
m-Ni-BMF-N-C	-1.1	~12.5	0.1 M $KHCO_3$	17
Ni-N_3/Cr-N_2	-0.8	27.3	0.5 M $KHCO_3$	18
Ni_2-NCNT	-0.9	~30	0.5 M $KHCO_3$	19
NiFe-DASC	-0.8	50.4	0.5 M $KHCO_3$	20
NiZn-N_6-C	-0.9	20.2	0.5 M $KHCO_3$	21
Fe_2-N-C	-1.06	~21.0	0.5 M $KHCO_3$	22
Ni/NC_{S-260}	-0.8	42.8	0.5 M $KHCO_3$	This work

Reference

1. C. Zhang, B. Miao and Z Zhao, *J. Mater. Chem. A*, 2026, **14**, 12107-12115.
2. W. Zhang, A. Mehmood, G. Ali, H. Liu, L. Chai, J. Wu and M. Liu, *Angew. Chem. Int. Ed.*, 2025, **64**, e202424552.
3. Z. Zhu, W. Tang, X. Huang, J. Wang, X. Niu, J. Chen, B. Liu, R. Wu and Z. Wei, *CCS Chem.*, 2026.
4. J. Wang, Y. Sun, M. Li, Y. Yi, Q. Liu, Z. Li and L. Wang, *Nano Lett.*, 2025, **25**, 8168-8175.
5. C. Wang, B. Chen, H. Ren, X. Wang, W. Li, H. Hu, X. Chen, Y. Liu, Q. Guan and W. Li, *App. Catal. B: Environ.*, 2025, **368**, 125151.
6. F. Wang, G. Wang, P. Deng, Y. Chen, J. Li, D. Wu, Z. Wang, C. Wang, Y. Hua and X. Tian, *Small*, 2023, **19**, 2301128.
7. Y. Gong, C. Cao, W. Shi, J. Zhang, J. Deng, T. Lu and D. Zhong, *Angew. Chem. Int. Ed.*, 2022, **61**, e202215187.
8. J. Wu, W. Zhang, L. Wu, X. Wang, J. Yuan, K. Xu, Y. Hua, Z. Gao, H. Liu and M. Liu, *Angew. Chem. Int. Ed.*, 2026, **65**, e18107.
9. Q. Lu, C. Chen, Q. Di, W. Liu, X. Sun, Y. Yuo, Y. Zhou, Y. Pan, X. Feng, L. Li, D. Chen and J. Zhang, *ACS Catal.*, 2022, **12**, 1364-1374.
10. W. Sun, S. Liu, H. Sun, H. Hu, J. Li, L.Wei, Z. Tian, Q. Chen, J. Su and L. Chen, *Adv. Energy Mater.*, 2025, **15**, 2500283.
11. J. Niu, H. Li, Y. Li, D. Jia, N. Chen, H. Li, M. Liu, J. Qiu and X. He, *Carbon Energy*, 2025; e70112.
12. Z. Liu, L. Cao, M. Wang, Y. Zhao, M. Hou, and Z. Shao, *J. Mater. Chem. A*, 2024, **12**, 8331-8339.
13. S. Zhang, P. Yue, Y. Zhou, J. Li, X. Zhu, Q. Fu and Q. Liao, *Small*, 2023, **19**, 2303016.
14. Y. Li, X. F. Lu, S. Xi, D. Luan, X. Wang, X. W. D. Lou, *Angew. Chem. Int. Ed.*, 2022, **61**, e202201491.
15. C. Jia, X. Tan, Y. Zhao, W. Ren, Y. Li, Z. Su, S. Smith and C. Zhao, *Angew. Chem. Int. Ed.*, 2021, **60**, 23342-23348.
16. J. Cho, J. Ma, C. Lee, J. Lim, Y. Kim, H. Jang, J. Kim, M. Seo, Y. Choi, Y. Jang, S. Ahn, H. Jang, S. Back, J. Lee and S. Kim, *Carbon Energy*, 2024, **6**, e510.
17. Y. Lee, B. Park, S. You, C. Lim, K. Cho, D. Lee, C. Jo, W. Kim, K. Lee, Y. Kim, H. Oh and J. Han, *Nano Energy*, 2026, **152**, 111880.
18. H. Fu, M. Zhou, T. Yu, Y. Yang, J. Sun, N. Bedford, L. Wang, P. Liu, C. Lian, H. Wang, H. Yang and H. Zhao, *Angew. Chem. Int. Ed.*, 2025, e21247.
19. X. Liang, H. Wang, C. Zhang, D. Zhong, and T. Lu, *Appl. Catal. B-Environ.*, 2022, **322**, 122073.
20. Z. Zeng, L. Y. Gan, H. Bin Yang, X. Su, J. Gao, W. Liu, H. Matsumoto, J. Gong, J. Zhang, W. Cai, Z. Zhang, Y. Yan, B. Liu, and P. Chen, *Nat. Commun.*, 2021, **12**, 4088.
21. Y. Li, B. Wei, M. Zhu, J. Chen, Q. Jiang, B. Yang, Y. Hou, L. Lei, Z. Li, R. Zhang, and Y. Lu, *Adv. Mater.* 2021, **33**, 2102212.
22. Y. Wang, B. J. Park, V. K. Paidi, R. Huang, Y. Lee, K. Noh, K. Lee, and J. Han, *ACS Energy Lett.*, 2022, **7**, 640.